



Direct and cascaded collective third-harmonic generation in metasurfaces

OFER DORON,^{1,2,3,*} LIOR MICHAELI,^{1,2,3} AND TAL ELLENBOGEN^{1,3}

¹Faculty of Engineering, Department of Physical Electronics, Tel Aviv University, Tel Aviv 69978, Israel

²Raymond and Beverly Sackler School of Physics & Astronomy, Tel Aviv University, Tel Aviv 69978, Israel

³Tel Aviv Center for Light-Matter Interaction, Tel Aviv University, Tel Aviv 69978, Israel

*Corresponding author: oferdoron@mail.tau.ac.il

Received 11 February 2019; revised 14 May 2019; accepted 21 May 2019; posted 21 May 2019 (Doc. ID 359927); published 14 June 2019

We use collective interactions in plasmonic metasurfaces to manipulate the interplay between direct and cascaded third-harmonic generation. We implement a simple case where in contrast to the direct contribution, which is mainly enhanced by the local plasmonic resonances, the cascaded contribution enhancement may be manipulated using the metasurface's geometry, in addition to the single nanoparticle's electrical response, by enabling the proper nonlocal interactions at the second-harmonic frequency. In addition, an anomalous phase relation of the single nanoparticle's linear polarizability at the second-harmonic region affects the relative phase between the direct and cascaded contributions, which results in a Fano-like asymmetrical line shape of the third-harmonic generation. We demonstrate that this can be used to enhance or contrarily completely eliminate third-harmonic generation from metasurfaces over a very narrow bandwidth. Such a unique fundamental observation of the interplay between direct and cascaded third-harmonic generation in periodic resonant systems may find new applications in sensing and to control nonlinear optical phenomena. © 2019 Optical Society of America

<https://doi.org/10.1364/JOSAB.36.000E71>

1. INTRODUCTION

Coherent collective scatterings in metallic nanoparticle (NP) arrays has been investigated in recent years, in both the linear and nonlinear regimes [1–4]. Frequently, the coupled dipole approximation (CDA) is used to model and analyze the array response. Hybridization of the local plasmonic mode of the NPs, known as localized surface plasmon resonance (LSPR), with the nonlocal photonic mode of the array, which arise when coherent scattering takes place under the Rayleigh anomaly (RA) condition, creates a surface lattice resonance (SLR). SLRs show sharp spectral features and an enhanced electric field response compared to the LSPR of the single NP [5–7]. These attributes make them useful for many processes and applications, which include tunable lasing [8–10], ultra-narrowband absorbers [11], coupling of bright and dark modes [12], directional emission of polarized light [13], and enhanced electron photoemission in photodetectors [14].

In addition, enhancement of second-harmonic generation (SHG) from plasmonic arrays was achieved using linear [15] and nonlinear [16] RAs [i.e., coherent scatterings at either the fundamental frequency (FF) or the second harmonic (SH)]. These observations were phenomenologically explained by Michaeli *et al.*, by extension of the conventional CDA to the nonlinear case [16]. Moreover, coherent scattering at the SH was shown by simulation to also enhance third-harmonic

generation (THG) by means of cascaded THG [17]. As opposed to direct THG, which converts three FF photons into a third harmonic (TH) photon through the material's cubic nonlinearity, cascaded THG may occur in quadratic nonlinear materials and rises from a SHG process followed by a sum-frequency generation (SFG) involving the SH and the FF waves. Conventional schemes to control these two separate THG mechanisms mostly rely on selective phase matching of the different processes (i.e., SHG, SFG, or THG) [18–20]. In two-dimensional (2D) structures, such as NP arrays and metasurfaces, a longitudinal phase-matching condition is irrelevant. However, adequately spacing the NPs in the array may result in the coherent scattering of light, which acts as an analog to the phase-matching condition.

In this work, we demonstrate control over the effective cubic nonlinearity of plasmonic NP arrays. In addition to enhancement of the cascaded THG process that can be achieved by the presence of SLR at the SH [17], we show that the interplay between direct and cascaded THG may lead to constructive and destructive interference in very close spectral proximity. An anomalous phase relation of the single NP's polarizability, which exists around the SH, plays a crucial role in adjusting the phase of the cascaded contribution to the THG. Specifically, it enables a rapid phase change of the cascaded process compared to the direct contribution, which leads to constructive and destructive interference in very close spectral proximity.

As a result, the total THG manifests in a Fano-like asymmetrical line shape with enhancement or complete elimination points.

2. COUPLED DIPOLE APPROXIMATION

To capture the dynamics of an array of NPs, we must consider the impinging field as well as the scattered fields by the NPs. The CDA is commonly used in this case. The model describes all the NPs in the array as point dipoles. The induced dipole moment at the i^{th} lattice point is proportional to the local electric field through

$$p_i(\omega) = \alpha_{i,s}(\omega)E_{i,\text{loc}}(\omega), \quad (1)$$

where $\alpha_{i,s}(\omega)$ is the frequency-dependent polarizability of the single NP at the i^{th} lattice point, which is enhanced at the LSPR. In addition, the scalar approximation was used, which assumes that the polarizability is a scalar and not a rank 2 tensor. As a result, all the induced dipole moments are in the same direction of the polarization of the impinging light.

Expressing the local field as the sum of the applied field and the scattered field yields

$$\begin{aligned} E_{i,\text{loc}}(\omega) &= E_{i,\text{app}}(\omega) + E_{i,\text{sca}}(\omega) \\ &= E_{i,\text{app}}(\omega) + \sum_{j \neq i} A_{ij}(\omega)p_j(\omega), \end{aligned} \quad (2)$$

where A_{ij} is the Green's function of a dipole describing scattering from the j^{th} dipole to the i^{th} dipole. Under the scalar approximation, the Green's function takes the form

$$A_{ij}(\omega) = e^{ikr_{ij}} \left[\frac{(1 - ikr_{ij})(3 \cos^2(\theta_{ij}) - 1)}{r_{ij}^3} + \frac{k^2 \sin^2(\theta_{ij})}{r_{ij}} \right], \quad (3)$$

where \mathbf{r}_{ij} is the distance vector between i^{th} the j^{th} dipoles, θ_{ij} is the angle between the impinging light's polarization and \mathbf{r}_{ij} , $k = n(\omega)\omega/c$ is the wave vector of illumination angular frequency ω , $n(\omega)$ is the refractive index, and c is the speed of light.

The terms in the scattering sum in Eq. (2) are summed constructively under the RA condition, when a diffraction order of the array propagates on the array plane. The RA condition may be understood through the conservation of quasimomentum as

$$\mathbf{k}_{\parallel} + \mathbf{G}_{m_1, m_2} = \mathbf{k}_s, \quad (4)$$

where \mathbf{k}_{\parallel} is the component of the illumination wave vector parallel to the array surface, $\mathbf{G}_{m_1, m_2} = m_1\mathbf{b}_1 + m_2\mathbf{b}_2$ is a general reciprocal lattice vector with $m_1, m_2 \in \mathbb{Z}$, \mathbf{b}_1 and \mathbf{b}_2 are the primitive reciprocal lattice vectors, and \mathbf{k}_s is the wave vector of the surface scattered wave.

Equations (1)–(3) are a set of self-consistent equations for the dipole moments in the array. It is instructive to study the case of an infinite array under illumination at normal incidence and to obtain an analytical expression for the solution. In this case, one may drop the indices in Eqs. (1) and (2) as a result of the translation symmetry of the lattice. The infinite summation over all the Green's functions yields the array's structural factor,

$$S(\omega) = \sum_{j \neq 0} A_{0j}(\omega). \quad (5)$$

The structural factor describes the collective contribution of the array's photonic modes and is defined for illumination at normal incidence. In general, for illumination at oblique incidence, the structural factor may be defined to depend on the in-plane momentum of the impinging light \mathbf{k}_{\parallel} [21], but for the case of illumination at normal incidence this dependence is null. The dipoles are driven in phase and thus the in-plane momentum may be ignored. For the simple case of illumination at normal incidence on a 1D infinite chain, the infinite scattering sum is summed constructively according to Eq. (3) under the condition

$$kd = 2\pi m, \quad (6)$$

where d is the chain's spacing and $m \in \mathbb{N}$. This condition of coherent scattering coincides with the RA condition from Eq. (4) with $\mathbf{k}_{\parallel} = 0$.

Solving Eqs. (1)–(3) and (5) to find the effective polarizability, associated with the applied field rather than the local field $p(\omega) = \alpha_{\text{eff}}(\omega)E_{\text{app}}(\omega)$, under illumination at normal incidence results in

$$\alpha_{\text{eff}}(\omega) = \frac{\alpha_s(\omega)}{1 - S(\omega)\alpha_s(\omega)}. \quad (7)$$

The effective polarizability accounts for the lattice interactions through the structural factor. Moreover, the effective polarizability describes the formation of SLRs under the condition that both $\alpha_s(\omega)$ and $S(\omega)$ are resonant simultaneously (i.e., when the LSPR of the single NP and the RA of the array share the same spectral region).

Now we implement the nonlinear CDA described in [16,17] for the case of THG to calculate the effective second-order hyperpolarizability of an infinite array under illumination at normal incidence under the non-depleted pump approximation. The first- and second-order hyperpolarizabilities associate the induced dipole moment to the square and cube of the local electric field, respectively. We use the scalar approximation for the hyperpolarizabilities, which means that the induced dipole moment is in the same direction for all harmonics. As in the linear case, the effective second-order hyperpolarizability is related to the applied field rather than the local field, $p(3\omega) = (1/3!)\gamma_{\text{eff}}^3 E_{\text{app}}^3(\omega)$.

We start by writing the induced dipole moment at the SH [16] as

$$p(2\omega) = \frac{1}{2!}\beta_s^{(\text{SHG})} E_{\text{loc}}^2(\omega) + \alpha_s(2\omega)E_{\text{loc}}(2\omega), \quad (8)$$

where $\beta_s^{(\text{SHG})} \equiv \beta_s(2\omega; \omega, \omega)$ is the single NP's first-order SHG hyperpolarizability. To enable second-order interactions (i.e., $\beta_s \neq 0$), the NPs are assumed to break inversion symmetry along the induced dipole moment. The first term describes the SHG process where the FF local field is calculated from Eq. (2). This local field accounts for the scattered field in addition to the applied field and therefore may be enhanced under the RA condition. The second term contains the local field at the SH that each dipole experiences. This field results from the sum of scattered fields, $E_{\text{loc}}(2\omega) = E_{\text{sca}}(2\omega)$.

Next, we write the induced dipole moment at the TH as

$$p(3\omega) = \frac{1}{3!}\gamma_s^{(\text{THG})}E_{\text{loc}}^3(\omega) + \beta_s^{(\text{SFG})}E_{\text{loc}}(\omega)E_{\text{loc}}(2\omega) + \alpha_s(3\omega)E_{\text{loc}}(3\omega), \quad (9)$$

where $\beta_s^{(\text{SFG})} \equiv \beta_s(3\omega; 2\omega, \omega)$ and $\gamma_s^{(\text{THG})} \equiv \gamma_s(3\omega; \omega, \omega, \omega)$ are the single NP's first-order SFG and second-order THG hyperpolarizabilities, respectively. The first term describes the direct THG process and the second term describes the collective cascaded THG process. For simplicity, self-cascading effects have been neglected. It is possible to model such effects directly into the single NP's second-order hyperpolarizability— $\gamma_s^{(\text{THG})}$. The third term contains the local field at the TH and, as for the SH case in Eq. (8), this term describes the scattering at the TH as $E_{\text{loc}}(3\omega) = E_{\text{sca}}(3\omega)$.

The local field at the harmonics, 2ω and 3ω , takes the form

$$E_{\text{loc}}(m\omega) = E_{\text{sca}}(m\omega) = \sum_{j \neq 0} A_{0j}(m\omega)p(m\omega) = S(m\omega)p(m\omega), \quad (10)$$

where $m \in \{2, 3\}$. The structural factors at the harmonics describe the sum of the scattered fields from all the other dipoles in the array. The structural factors become resonant under the nonlinear RA condition where a diffraction order of the relevant harmonic propagates on the surface. For the case of a 1D chain under illumination at normal incidence this condition has the form of Eq. (6), using the k -vector of the relevant harmonic instead of the FF k -vector, and describes coherent scattering on the chain axis at the chosen harmonic. For oblique incidence, the full nonlinear, quasimomentum matching conditions on the surface must be considered to find the nonlinear RA condition [16].

Solving Eqs. (1)–(3) and (5) along with Eqs. (8)–(10) to find the effective second-order hyperpolarizability yields (see Appendix A for full derivation)

$$\gamma_{\text{eff}} = \gamma_{\text{direct}} + \gamma_{\text{cas}} = \frac{\gamma_s^{(\text{THG})} + 3\beta_s^{(\text{SFG})}\beta_s^{(\text{SHG})}\frac{S(2\omega)}{1-\alpha_s(2\omega)S(2\omega)}}{(1-\alpha_s(\omega)S(\omega))^3(1-\alpha_s(3\omega)S(3\omega))}. \quad (11)$$

The effective second-order hyperpolarizability accounts for lattice effects through the structural factors at all harmonics and is an exact expression that describes the whole array response with nontrivial dependency on the model's parameters. It can be seen that the effective hyperpolarizability is separated into its two contributions, the direct and the cascaded. Both contributions share the same denominator, which may become resonant under the linear and TH nonlinear SLRs. The main difference between the two contributions in Eq. (11) is the array's structural factor at the SH [$S(2\omega)$], which appears only in the cascaded term. Moreover, $S(2\omega)$ appears in the numerator of the cascaded term in addition to its denominator, giving the option for enhancement of this term at the SH nonlinear RA condition (i.e., even if the single particle is not resonant at the SH). Since $S(2\omega)$ is dependent on the array geometry, while the LSPR is not, the cascaded term can be further manipulated compared to the direct term. In general, the two contributions

to the THG may sum up constructively to enhance the total THG or destructively to reduce or even eliminate the THG. The above findings are equally valid for 1D chains and 2D arrays. To demonstrate, in the next section we present numerical results based on 1D chains.

3. SIMULATIONS

To study the nonlinear dynamics and the interplay between the direct and cascaded terms in a simple system, we implemented the nonlinear CDA on an infinite 1D chain of nonlinear dipoles under illumination at normal incidence. The simulated chain is illustrated in Fig. 1. The spacing of the chain was taken to be $d = 660$ nm and the surrounding refractive index $n = 1.51$ to support SH nonlinear RA at $\lambda_{FF} = 2nd \approx 1990$ nm. The applied field is polarized perpendicular to the chain's direction and induces the dipole moments in the same direction for all harmonics.

A single LSPR of the NPs can be approximated as a Lorentzian of the form [22]

$$\alpha_s(\omega, \omega_{\text{res}}) = \frac{A}{\omega_{\text{res}} - \omega + i\gamma}, \quad (12)$$

where A is the polarizability amplitude, $\omega_{\text{res}} = 2\pi c/\lambda_{\text{res}}$ is the resonance frequency, λ_{res} is the resonance free-space wavelength, and γ is the damping constant. We consider the case where each NP has two resonances at $\lambda_{\text{res},1} = 2000$ nm and $\lambda_{\text{res},2} = 700$ nm with damping constants of $\gamma_1 = 1.38 \times 10^{14}$ Hz and $\gamma_2 = 1.69 \times 10^{14}$ Hz, respectively. The damping constants were chosen to be the same order of magnitude as in [23]. Such double resonance behavior can be found, for example, in [24,25]. In this case, the single NP's polarizability can be represented as the sum of the two Lorentzian functions with different amplitudes,

$$\alpha_s(\omega) = A_1\alpha_s(\omega, \omega_{\text{res},1}) + A_2\alpha_s(\omega, \omega_{\text{res},2}). \quad (13)$$

Assuming that the single NP may be modeled as an anharmonic oscillator [26], with quadratic and cubic restoring forces, the nonlinear hyperpolarizabilities may be expressed according to Miller's rule [27,28] as

$$\begin{aligned} \beta_s^{(\text{SHG})} &= B_1\alpha_s^2(\omega)\alpha_s(2\omega), \\ \beta_s^{(\text{SFG})} &= B_2\alpha_s(\omega)\alpha_s(2\omega)\alpha_s(3\omega), \\ \gamma_s^{(\text{THG})} &= C\alpha_s^3(\omega)\alpha_s(3\omega), \end{aligned} \quad (14)$$

where B_1 , B_2 , and C are constants.

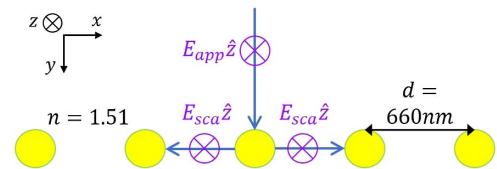


Fig. 1. Schematic illustration of the infinite 1D chain used in the simulation with a spacing of $d = 660$ nm and a surrounding medium refractive index of $n = 1.51$. The impinging and scattered light are marked by blue arrows in the y - and x -directions, respectively, and their polarization is displayed in purple in the z -direction. The dipole moments are induced in the z -direction and emit the scattered light along the chain's axis.

The amplitude constants of the polarizability and hyperpolarizabilities in the simulations were chosen similarly to [17] to be $A_1 = 0.3 \text{ cm}^3 \text{ s}^{-1}$, $A_2 = 0.2 \text{ cm}^3 \text{ s}^{-1}$, $B_1 = B_2 = 5 \times 10^{-9} \text{ nm}^{-5} \text{ V}^{-1}$, and $C = 10^{-12} \text{ nm}^{-7} \text{ V}^{-2}$. The hyperpolarizability constants B_1, B_2, C were chosen such that the off-resonance values of the single NP's hyperpolarizabilities, $\beta_s^{(\text{SHG})}, \beta_s^{(\text{SFG})}, \gamma_s^{(\text{THG})}$ are of the same order of magnitude as in [17].

The nonlinear simulations were done for fundamental wavelength range of $\lambda_{\text{FF}} = 1500\text{--}2500 \text{ nm}$ with the main area of interest around $\lambda_{\text{FF}} \approx 2000 \text{ nm}$, where the two contributions to the THG are resonant. The SH and TH ranges for the simulation are $750\text{--}1250 \text{ nm}$ and $500\text{--}833 \text{ nm}$, respectively.

Figure 2(a) depicts the absolute value (blue solid line) and phase (red dashed line) of the single NP's linear polarizability as a function of the FF wavelength. The polarizability is resonant at the FF ($\sim 2000 \text{ nm}$) and the TH ($\sim 666 \text{ nm}$) and nonresonant for the SH wavelengths range ($\sim 1000 \text{ nm}$). Looking at Eq. (14), we see that the single NP's first-order hyperpolarizabilities are not significantly enhanced under these conditions compared to the second-order hyperpolarizability. Therefore, the direct contribution is dominant in this case.

The phase of a single LSPR experiences a positive change of π from the shorter wavelengths to longer ones. The proximity of the two resonances creates a special phase behavior: Near each resonance the phase rises in accordance to a single LSPR. However, in-between the two resonances, at the SH range, the phase drops. Such an anomalous phase relation is associated to many phenomena, including electromagnetic-induced transparency [29,30], slow light [31], superluminal

light [32], and tunable all-optical delays in optical fibers [33]. In this case, the anomalous phase is expressed, according to Eq. (14), in the first-order hyperpolarizabilities and affects the phase of cascaded THG process compared to the direct process. Hence, it enables an interesting interplay between the two contributions to the THG.

Figure 2(b) depicts the absolute value (blue solid line) and phase (red dashed line) of the structural factor at the SH, $S(2\omega)$, as a function of the FF wavelength, λ_{FF} (bottom axis), and the SH wavelength, λ_{SH} (top axis). The absolute value shows a sharp peak at $\lambda_{\text{FF}} \approx 1990 \text{ nm}$ ($\lambda_{\text{SH}} \approx 995 \text{ nm}$). Note that this sharp feature is not due to the linear interaction of FF with the structure, but because of the nonlinear scattering of the SH, where the nonlinear SH RA condition is fulfilled. The nonlinear RA wavelength corresponds to the first order RA of the SH and can be found using Eq. (6) with the k -vector of the SH and $m = 1$. This strong resonance is translated to a cascaded THG enhancement, according to Eq. (11). The phase of $S(2\omega)$ experiences a change of over a π in the simulation range from $\varphi \approx 0.8\pi$ to $\varphi \approx -0.5\pi$, with an abrupt drop of almost $\pi/2$ over a 100 nm bandwidth. In addition, the abrupt drop occurs while crossing the nonlinear RA, where the phase φ is around zero. Higher orders of nonlinear RAs exist for $m > 1$ in Eq. (6), but the nearest RA is at $\lambda_{\text{FF}} \approx 1000 \text{ nm}$ ($\lambda_{\text{SH}} \approx 500 \text{ nm}$), which is out of the relevant range of this simulation— $1500 \text{ nm} < \lambda_{\text{FF}} < 2500 \text{ nm}$ ($750 \text{ nm} < \lambda_{\text{SH}} < 1250 \text{ nm}$).

In Fig. 3(a) the absolute value of the direct (blue solid line), cascaded (red dashed line), and total (yellow dotted line) effective second-order hyperpolarizabilities from Eq. (11) are depicted as a function of the FF wavelength, λ_{FF} (bottom axis), and the generated TH wavelength, λ_{TH} (top axis). Both the direct and cascaded contributions to the THG are resonant around $\lambda_{\text{FF}} \approx 2000 \text{ nm}$ ($\lambda_{\text{TH}} \approx 667 \text{ nm}$). The spectrally broad resonant response of the direct contribution originates from the LSPRs and the spectrally narrow resonant response of the cascaded contribution is caused by the photonic mode of the lattice.

In contrast to both of its contributions, the total THG is highly asymmetric and shows a Fano-like spectral line shape. On the long wavelengths side, the two contributions add up constructively to increase the total THG. On the short wavelength side, the two contributions interfere destructively and exhibit THG elimination. The vertical dashed-dotted lines in Fig. 3(a) mark the wavelengths of destructive and constructive interference.

To understand the different interference cases, it is useful to look at Fig. 3(b), which depicts the phase of the direct (blue solid line), cascaded (red dashed line), and total (yellow dotted line) effective second-order hyperpolarizabilities from Eq. (11) as a function of the FF wavelength, λ_{FF} (bottom axis), and the generated TH wavelength, λ_{TH} (top axis). Figure 3(c) shows the direct, cascaded, and total hyperpolarizabilities at the two wavelengths marked in Figs. 3(a) and 3(b) on the complex plane. The phase difference between the direct and cascaded terms on the right side of the resonance is approximately $7\pi/4$, which leads to constructive interference, as shown in Fig. 3(c) for $\lambda_{\text{FF}} = 2060 \text{ nm}$ ($\lambda_{\text{TH}} \approx 687 \text{ nm}$), where the

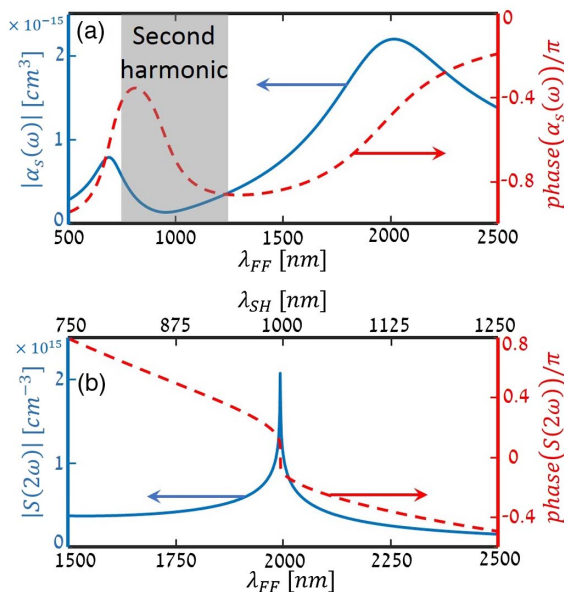


Fig. 2. (a) Absolute value (blue solid line) and phase (red dashed line) of the single particle polarizability. The polarizability possesses two resonances at $\lambda_{\text{res},1} = 2000 \text{ nm}$ and $\lambda_{\text{res},2} = 700 \text{ nm}$. The grey area shows the SH region of the simulation. (b) Absolute value (blue solid line) and phase (red dashed line) of the structural factor at the SH as a function of the FF wavelength (bottom axis) and the SH wavelength (top axis). The structural factor features a sharp enhancement at $\lambda_{\text{FF}} \approx 1990 \text{ nm}$ ($\lambda_{\text{SH}} \approx 995 \text{ nm}$) under the nonlinear RA condition.

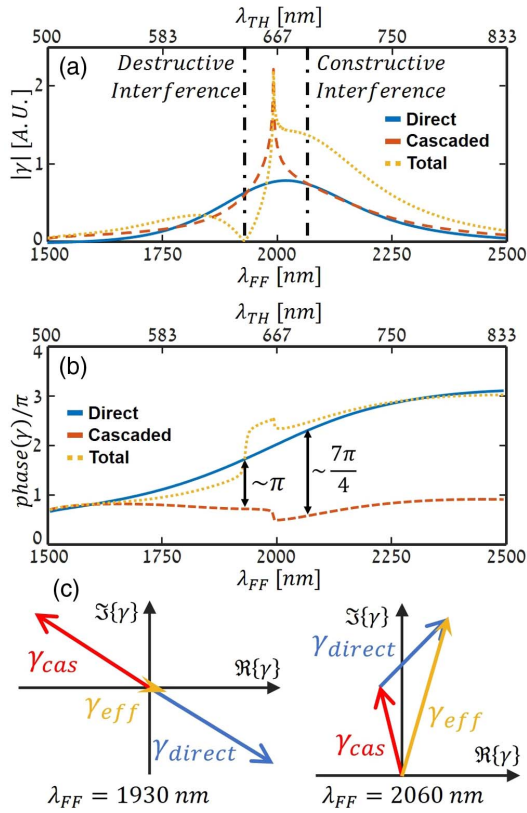


Fig. 3. (a) Absolute value and (b) phase of the direct (blue solid line), cascaded (red dashed line) and total (yellow dotted line) effective second-order hyperpolarizability as a function of the FF wavelength (bottom axis) and TH wavelength (top axis), calculated from Eq. (11). The black vertical dash-dotted lines in (a) and the black vertical arrows in (b) correspond to wavelengths of $\lambda_{FF} = 1930$ nm and $\lambda_{FF} = 2060$ nm. (c) The direct (blue arrow), cascaded (red arrow), and total (yellow arrow) effective hyperpolarizabilities for the two wavelengths marked in (a)–(b) on the complex plane show both destructive (left) and constructive (right) interference.

two contributions add up to almost double their original value. On the left side of the resonance, the phase difference is approximately π , which leads to destructive interference, as shown in Fig. 3(c) for $\lambda_{FF} = 1930$ nm ($\lambda_{TH} \approx 643$ nm), where the total THG is eliminated.

The source of this quickly varying phase difference from π for destructive interference to $\sim 7\pi/4$ for constructive interference is the anomalous phase of the polarizability at the SH region superimposed with the sudden phase jump of the SH structural factor at the RA wavelength. The phase difference between the cascaded and direct second-order hyperpolarizabilities, $\Delta\Phi = \varphi_{cas} - \varphi_{direct}$, can be calculated from their ratio,

$$\frac{\gamma_{cas}}{\gamma_{direct}} = \frac{3\beta_s^{(SFG)}\beta_s^{(SHG)}S(2\omega)}{\gamma_s^{(THG)}(1 - S(2\omega)\alpha_s(2\omega))} \approx \alpha_s^2(2\omega)S(2\omega), \quad (15)$$

where we used Miller's rule from Eq. (14) and the fact that $1 - S(2\omega)\alpha_s(2\omega)$ is almost constant in the relevant spectral regime to make the last step. This reveals that $\Delta\Phi$ depends on the phase of both the polarizability and the structural factor at the SH.

Table 1. Phase Difference between the Cascaded and Direct Hyperpolarizabilities^a

		$\alpha_s(2\omega)$	$\alpha_s^2(2\omega)$	$S(2\omega)$	$\Delta\Phi$
NP 1	λ_{DES}	$\sim -\pi$	$\sim 0.1\pi$	$\sim 0.25\pi$	$\sim 0.35\pi$
	λ_{CON}	$\sim -\pi$	$\sim 0.1\pi$	$\sim -0.2\pi$	$\sim -0.1\pi$
	$\delta\varphi$	~ 0	~ 0	$\sim 0.45\pi$	$\sim 0.45\pi$
NP 2	λ_{DES}	$\sim -0.6\pi$	$\sim -1.2\pi$	$\sim 0.25\pi$	$\sim -\pi$
	λ_{CON}	$\sim -0.75\pi$	$\sim -1.5\pi$	$\sim -0.2\pi$	$\sim -1.75\pi$
	$\delta\varphi$	$\sim 0.15\pi$	$\sim 0.3\pi$	$\sim 0.45\pi$	$\sim 0.75\pi$

^aNote: The phase of the polarizability $\alpha_s(2\omega)$, polarizability squared $\alpha_s^2(2\omega)$, and the structural factors $S(2\omega)$ at the SH and the phase difference between the cascaded and direct contributions $\Delta\Phi$ for the original destructive ($\lambda_{DES} = 1930$ nm) and constructive ($\lambda_{CON} = 2060$ nm) interference wavelengths, which are marked in Fig. 3, for the two NPs. In addition, the change of the phase between the two wavelengths, $\delta\varphi$, is shown for each considered quantity.

To examine the effect of the anomalous phase of the single NP on $\Delta\Phi$, we simulated the response of two identical chains as in Fig. 1, which only differ by the composing individual NP. The first NP type (NP 1) possesses one resonance at the FF wavelength— $\lambda_{res} = 2000$ nm. The polarizability therefore takes the form of Eq. (12) and lacks the anomalous phase relation. The second NP type (NP 2) is identical to the NP depicted in Fig. 2(a), which possesses two resonances at the FF and TH wavelengths and retains the anomalous phase relation at the SH region. Figure 4 shows $\Delta\Phi$ for the two NP types, with one (NP 1, blue solid line) or two (NP 2, red dotted line) resonances as a function of the FF wavelength, λ_{FF} (bottom axis), and the TH wavelength, λ_{TH} (top axis). In addition, Table 1 shows the phase of $\alpha_s(2\omega)$, $\alpha_s^2(2\omega)$, and $\Delta\Phi$ for the destructive and constructive interference wavelengths marked in Fig. 4, as well as the phase change between the two wavelengths, marked $\delta\varphi$.

According to Fig. 4 and Table 1, it is apparent that the phase difference $\Delta\Phi$ of the NP 1 chain is almost identical to the phase

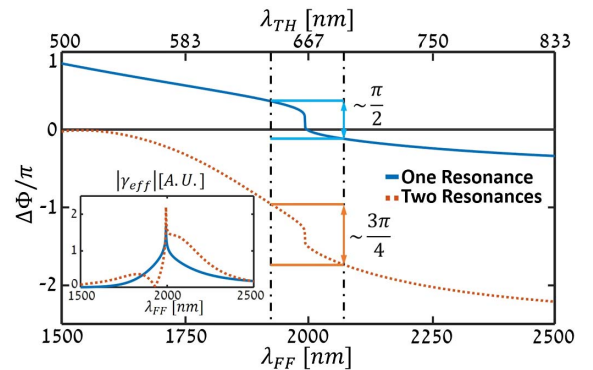


Fig. 4. Phase difference between the cascaded and direct second-order hyperpolarizabilities for NP 1 chain (blue solid line) and for NP 2 chain (red dotted line) as a function of the FF wavelength (bottom axis) and TH wavelength (top axis), calculated as the phase of the ratio in Eq. (15). The dotted grey vertical lines mark the wavelength of destructive ($\lambda_{DES} = 1930$ nm) or constructive ($\lambda_{CON} = 2060$ nm) interference, respectively. The light blue and orange arrows show the phase difference change between the destructive and constructive interference wavelengths (i.e., $\delta\varphi$) in Table 1. The inset shows the absolute value of effective second-order hyperpolarizabilities for the two NP types.

of $S(2\omega)$, with only small deviations. The phase of $\alpha_s^2(2\omega)$, which adds to the phase of $S(2\omega)$ to give $\Delta\Phi$, does not greatly change the phase of $S(2\omega)$, as can be seen quantitatively from Table 1. Thus, the SH polarizability does not play a significant role in shaping the NP 1 chain phase difference. In this case, at both wavelengths of the original destructive and constructive interference $\Delta\Phi$ describes constructive interference between the cascaded and direct THG. The absolute value of the effective second-order hyperpolarizability for NP 1 (blue solid line) and NP 2 (red dotted line) is depicted in the inset of Fig. 4, which shows that on both sides of the NP 1 line shape the two contributions interfere constructively. The NP 2 line shape is identical to that in Fig. 3(a) and is shown for comparison with NP 1.

The phase of the NP 2 polarizability changes by the significant amount of $\sim 0.5\pi$ at the SH region, as can be seen from Fig. 2(a). It is apparent from Fig. 4 and Table 1 that between the destructive and constructive wavelengths, the phase of $\alpha_s^2(2\omega)$ adds to the phase of $S(2\omega)$ and shifts down the center of $\Delta\Phi$ at about 1.5π to the vicinity of $-\pi$, which enables destructive interference. In addition, $\Delta\Phi$ experiences a greater change upon crossing the nonlinear RA wavelength ($\lambda_{\text{FF}} \approx 1990$ nm) compared to the NP 1 chain, $3\pi/4$ versus $\pi/2$. The anomalous phase relation of $\alpha_s(2\omega)$ joins the descending phase of $S(2\omega)$ to increase the accessible $\Delta\Phi$ range before and after the nonlinear RA. $\Delta\Phi$ obtains the value $-\pi$ left to the nonlinear RA and the rapid change in $\Delta\Phi$ allows constructive interference on the right of the nonlinear RA.

4. SUMMARY

In this work, we used the nonlinear CDA to study the interplay between direct and cascaded contributions to THG on a 2D infinite plasmonic array under illumination at normal incidence. The nonlinear CDA shows that the second-order hyperpolarizability is the sum of cascaded and direct terms. Both terms share a common denominator, which becomes resonant for the SLR condition of the FF or TH; however, only the cascaded term has an additional denominator that describes the formation of SLR of the SH. In addition, the cascaded term contains the structural factor in the numerator, thus enabling enhanced cascaded THG independent of the single NP's polarizability.

We simulated a simple case of a 1D infinite chain to test the effective second-order hyperpolarizability from Eq. (11), which is the result of the nonlinear CDA. We found that the direct and cascaded contributions may interfere either constructively or destructively, resulting in an enhancement or total elimination of the THG, respectively. In addition, we discovered that even though the NPs are not resonant at the SH, their phase in this spectral region can significantly affect the relative phase between the two contributions to the THG. We specifically show that the existence of an anomalous phase of the polarizability at the SH influences the first-order hyperpolarizabilities, which appear only in the cascaded term, thus creating a phase difference between the direct and cascaded contributions. Also taking into account the phase of the SH structural factor, which shows a descending tendency over the simulation range, results in an over 2π change of the phase difference in the simulation

region. Together, these contributions lead to the observed Fano-like spectral line shape of the total THG and transition from enhancement to elimination.

APPENDIX A: DERIVATION OF THE EFFECTIVE SECOND-ORDER HYPERPOLARIZABILITY OF AN INFINITE 2D ARRAY UNDER ILLUMINATION AT NORMAL INCIDENCE

Here we show the derivation of Eq. (11) in the main text. We start from Eq. (2) along with Eqs. (5) and (7) for illumination at normal incidence to find the local field at the fundamental frequency by

$$\begin{aligned} E_{\text{loc}}(\omega) &= E_{\text{app}}(\omega) + E_{\text{sca}}(\omega) = E_{\text{app}}(\omega) \\ &+ \sum_{j \neq 0} A_{0j}(\omega) p(\omega) = E_{\text{app}}(\omega) + S(\omega) p(\omega) \\ &= E_{\text{app}}(\omega) + S(\omega) \frac{\alpha_s(\omega)}{1 - S(\omega)\alpha_s(\omega)} E_{\text{app}}(\omega) \\ &= \frac{E_{\text{app}}(\omega)}{1 - S(\omega)\alpha_s(\omega)}. \end{aligned} \quad (\text{A1})$$

Now we write Eq. (8) of the second harmonic using Eqs. (10) and (A1) to get

$$p(2\omega) = \frac{1}{2!} \beta_s^{(\text{SHG})} \frac{E_{\text{app}}^2(\omega)}{(1 - S(\omega)\alpha_s(\omega))^2} + \alpha_s(2\omega) S(2\omega) p(2\omega). \quad (\text{A2})$$

Solving for $p(2\omega)$ yields

$$p(2\omega) = \frac{1}{2!} \beta_s^{(\text{SHG})} \frac{E_{\text{app}}^2(\omega)}{(1 - S(\omega)\alpha_s(\omega))^2 (1 - S(2\omega)\alpha_s(2\omega))}. \quad (\text{A3})$$

We continue to the third harmonic and write Eq. (9) using Eqs. (10) and (A1) to get

$$\begin{aligned} p(3\omega) &= \frac{1}{3!} \gamma_s^{(\text{THG})} \frac{E_{\text{app}}^3(\omega)}{(1 - S(\omega)\alpha_s(\omega))^3} \\ &+ \beta_s^{(\text{SFG})} \frac{E_{\text{app}}(\omega)}{1 - S(\omega)\alpha_s(\omega)} S(2\omega) p(2\omega) \\ &+ \alpha_s(3\omega) S(3\omega) p(3\omega). \end{aligned} \quad (\text{A4})$$

Solving for $p(3\omega)$ and substituting $p(2\omega)$ with Eq. (A3) yields

$$p(3\omega) = \frac{1}{3!} \frac{\gamma_s^{(\text{THG})} + 3\beta_s^{(\text{SFG})} \beta_s^{(\text{SHG})} \frac{S(2\omega)}{1 - S(2\omega)\alpha_s(2\omega)}}{(1 - S(\omega)\alpha_s(\omega))^3 (1 - S(3\omega)\alpha_s(3\omega))} E_{\text{app}}^3(\omega). \quad (\text{A5})$$

From here, it is easy to extract the effective second-order hyperpolarizability defined in $p(3\omega) = (1/3!) \gamma_{\text{eff}} E_{\text{app}}^3(\omega)$ by

$$\gamma_{\text{eff}} = \frac{\gamma_s^{(\text{THG})} + 3\beta_s^{(\text{SFG})} \beta_s^{(\text{SHG})} \frac{S(2\omega)}{1 - S(2\omega)\alpha_s(2\omega)}}{(1 - S(\omega)\alpha_s(\omega))^3 (1 - S(3\omega)\alpha_s(3\omega))}. \quad (\text{A6})$$

Funding. H2020 European Research Council (ERC) (715362); Ministry of Science, Technology and Space (81604).

REFERENCES

1. B. Augu e and W. L. Barnes, "Collective resonances in gold nanoparticle arrays," *Phys. Rev. Lett.* **101**, 143902 (2008).
2. V. Giannini, G. Vecchi, and J. G omez Rivas, "Lighting up multipolar surface plasmon polaritons by collective resonances in arrays of nanoantennas," *Phys. Rev. Lett.* **105**, 266801 (2010).
3. W. Zhou and T. W. Odom, "Tunable subradiant lattice plasmons by out-of-plane dipolar interactions," *Nat. Nanotechnol.* **6**, 423–427 (2011).
4. S. Linden, F. B. P. Niesler, J. F orstner, Y. Grynko, T. Meier, and M. Wegener, "Collective effects in second-harmonic generation from split-ring-resonator arrays," *Phys. Rev. Lett.* **109**, 015502 (2012).
5. Y. Chu, E. Schonbrun, T. Yang, and K. B. Crozier, "Experimental observation of narrow surface plasmon resonances in gold nanoparticle arrays," *Appl. Phys. Lett.* **93**, 181108 (2008).
6. B. Augu e and W. L. Barnes, "Diffractive coupling in gold nanoparticle arrays and the effect of disorder," *Opt. Lett.* **34**, 401–403 (2009).
7. A. D. Humphrey and W. L. Barnes, "Plasmonic surface lattice resonances on arrays of different lattice symmetry," *Phys. Rev. B* **90**, 075404 (2014).
8. A. Yang, T. B. Hoang, M. Dridi, C. Deeb, M. H. Mikkelsen, G. C. Schatz, and T. W. Odom, "Real-time tunable lasing from plasmonic nanocavity arrays," *Nat. Commun.* **6**, 6939 (2015).
9. T. K. Hakala, H. T. Rekola, A. I. V akev ainen, J. P. Martikainen, M. Ne ada, A. J. Moilanen, and P. T orm a, "Lasing in dark and bright modes of a finite-sized plasmonic lattice," *Nat. Commun.* **8**, 13687 (2017).
10. D. Wang, A. Yang, W. Wang, Y. Hua, R. D. Schaller, G. C. Schatz, and T. W. Odom, "Band-edge engineering for controlled multi-modal nanolasing in plasmonic superlattices," *Nat. Nanotechnol.* **12**, 889–894 (2017).
11. Z. Li, S. Butun, and K. Aydin, "Ultranarrow band absorbers based on surface lattice resonances in nanostructured metal surfaces," *ACS Nano* **8**, 8242–8248 (2014).
12. S. R. K. Rodriguez, A. Abass, B. Maes, O. T. A. Janssen, G. Vecchi, and J. G omez Rivas, "Coupling bright and dark plasmonic lattice resonances," *Phys. Rev. X* **1**, 021019 (2011).
13. S. R. K. Rodriguez, G. Lozano, M. A. Verschuuren, R. Gomes, K. Lambert, B. De Geyter, A. Hassinen, D. Van Thourhout, Z. Hens, and J. G omez Rivas, "Quantum rod emission coupled to plasmonic lattice resonances: A collective directional source of polarized light," *Appl. Phys. Lett.* **100**, 111103 (2012).
14. S. V. Zhukovsky, V. E. Babicheva, A. V. Uskov, I. E. Protsenko, and A. V. Lavrinenko, "Enhanced electron photoemission by collective lattice resonances in plasmonic nanoparticle-array photodetectors and solar cells," *Plasmonics* **9**, 283–289 (2014).
15. R. Czaplicki, A. Kiviniemi, J. Laukkanen, J. Lehtolahti, M. Kuitinen, and M. Kauranen, "Surface lattice resonances in second-harmonic generation from metasurfaces," *Opt. Lett.* **41**, 2684–2987 (2016).
16. L. Michaeli, S. Keren-Zur, O. Avayu, H. Suchowski, and T. Ellenbogen, "Nonlinear surface lattice resonance in plasmonic nanoparticle arrays," *Phys. Rev. Lett.* **118**, 243904 (2017).
17. M. J. Huttunen, P. Rasekh, R. W. Boyd, and K. Dolgaleva, "Using surface lattice resonances to engineer nonlinear optical processes in metal nanoparticle arrays," *Phys. Rev. A* **97**, 053817 (2018).
18. S. Zhu, Y. Zhu, and N. Ming, "Quasi-phase-matched third-harmonic generation in a quasi-periodic optical superlattice," *Science* **278**, 843–846 (1997).
19. Y. Takagi and S. Muraki, "Third-harmonic generation in a noncentrosymmetrical crystal: direct third-order or cascaded second-order process?" *J. Lumin.* **87–89**, 865–867 (2000).
20. Y. Sheng, S. M. Saltiel, and K. Koynov, "Cascaded third-harmonic generation in a single short-range-ordered nonlinear photonic crystal," *Opt. Lett.* **34**, 656–658 (2009).
21. F. J. Garc a de Abajo, "Colloquium: Light scattering by particle and hole arrays," *Rev. Mod. Phys.* **79**, 1267–1290 (2007).
22. S. Zou, N. Janel, and G. C. Schatz, "Silver nanoparticle array structures that produce remarkably narrow plasmon lineshapes," *J. Chem. Phys.* **120**, 10871–10875 (2004).
23. N. Liu, L. Langguth, T. Weiss, J. K astel, M. Fleischhauer, T. Pfau, and H. Giessen, "Plasmonic analogue of electromagnetically induced transparency at the Drude damping limit," *Nat. Mater.* **8**, 758–762 (2009).
24. X. Huang, I. H. El-Sayed, W. Qian, and M. A. El-Sayed, "Cancer cell imaging and photothermal therapy in the near-infrared region by using gold nanorods," *J. Am. Chem. Soc.* **128**, 2115–2120 (2006).
25. M. W. Klein, C. Enkrich, M. Wegener, and S. Linden, "Second-harmonic generation from magnetic metamaterials," *Science* **313**, 502–504 (2006).
26. M. Hentschel, T. Utikal, H. Giessen, and M. Lippitz, "Quantitative modeling of the third harmonic emission spectrum of plasmonic nanoantennas," *Nano Lett.* **12**, 3778–3782 (2012).
27. R. C. Miller, "Optical second harmonic generation in piezoelectric crystals," *Appl. Phys. Lett.* **5**, 17–19 (1964).
28. R. W. Boyd, *Nonlinear Optics* (Academic, 2008).
29. M. Fleischhauer, A. Imamoglu, and J. P. Marangos, "Electromagnetically induced transparency: Optics in coherent media," *Rev. Mod. Phys.* **77**, 633–673 (2005).
30. S. E. Harris, J. E. Field, and A. Imamoglu, "Nonlinear optical processes using electromagnetically induced transparency," *Phys. Rev. Lett.* **64**, 1107–1110 (1990).
31. A. H. Safavi-Naeini, T. P. M. Alegre, J. Chan, M. Eichenfield, M. Winger, Q. Lin, J. T. Hill, D. E. Chang, and O. Painter, "Electromagnetically induced transparency and slow light with optomechanics," *Nature* **472**, 69–73 (2011).
32. M. S. Bigelow, N. N. Lepeshkin, and R. W. Boyd, "Superluminal and slow light propagation in a room-temperature solid," *Science* **301**, 200–202 (2003).
33. Y. Okawachi, M. S. Bigelow, J. E. Sharping, Z. Zhu, A. Schweinsberg, D. J. Gauthier, R. W. Boyd, and A. L. Gaeta, "Tunable all-optical delays via Brillouin slow light in an optical fiber," *Phys. Rev. Lett.* **94**, 153902 (2005).